Dynamic Modelling of the Aluminium Smelting Cell Mass and Energy Balance

Vanderlei Gusberti[(1)], Dagoberto S. Severo[(1)], Barry J. Welch[(2)], Maria Skyllas-Kazacos[(2)].

1) CAETE Engenharia, Rua Caeté 162, Porto Alegre RS– Brazil
caete@caetebr.com
2) School of Chemical Engineering, University of New South Wales, Sydney, NSW, 2052, Australia

Keywords: Reduction cell modelling, mass balance, heat balance, dynamic modelling, ledge movement.

Abstract

The understanding and quantification of the transient thermal behaviour of the Hall-Héroult cell is a key factor towards the improvement of the state-of-the-art of the aluminium smelting efficiency. Thermal disturbances in the present cell technology are unavoidable as consumable anodes, alumina and AlF_3 are added batchwise. Cell heat losses and bath chemistry are linked by the ledge solidification front dynamics.

This article presents a dynamic model of the mass and energy balance of aluminium smelting cells. A moving grid Finite Volume algorithm was developed to track the ledge movement coupled with a mass and energy balance model.

The dynamic model was applied to study the impact of mass and energy imbalances on the Hall-Héroult cell behaviour such as intermittent aluminium fluoride additions and several power modulation functions, which is a strategy used in some smelters in order to reduce overall energy costs.

The dynamic model is capable of using real cell mass and energy input history (such as current, voltage, alumina and fluoride addition rates) to predict the cell transient thermal response. The model results were compared with measurements obtained from industrial cells.

Introduction

In modern operation of aluminium electrolysis cells, the energy management and power consumption minimisation are key factors for the preservation of the smelter competitiveness. Quantifying and understanding the impact of disturbing actions in the cell energy balance is a path to improve process energy efficiency.
Numerical models that solve the cell energy balance for averaged steady state situation are commonly found in the literature [1-2]. However, the steady state thermal condition is never achieved in an industrial aluminium reduction cell. The prediction of transient cycles of the cell dynamics is very important in fine tunning the cell operation. It is during the cell thermal excursions that important inefficiencies and higher energy losses occur in the process. Advances in this field can be found in the literature [3-8]. In the dynamic model presented in this article, both mass and energy balances are calculated as a function of time, including evaluation of ledge thickness, bath volume and composition.

Mass Imbalances *versus* Energy Imbalances

Because the liquid bath is protected by a frozen bath layer, the cell thermal equilibrium is strongly linked to the cell mass stream equilibrium. During the cell operation, both equilibriums are periodically disturbed by actions such as anode change, metal tapping, fluoride additions, electrical power input changes, alumina feeding and others.

One example of the interacting heat and mass imbalances occurs when AlF_3 is added by cell operation in order to compensate for the cell AlF_3 consumption and to bring the bath composition back to the desired targets. Such correction in the bath composition causes a cascade of events in the cell thermal behaviour that may take hours or even days to stabilise. In a first moment after the fluoride addition, the AlF_3 concentration in the bath increases, the melting temperature of the bath decreases, superheat increases and a certain amount of ledge starts to melt down. This reduces the thermal resistance of the sidewall, increasing heat losses. After some time the bath temperature also decreases due to higher heat loss through the cell walls. Because the ledge presents a nearly eutectic cryolite composition ($3NaF \bullet AlF_3$), when it melts the AlF_3 concentration in the bath is lowered and the effect of the original addition is reduced. At some point, the new equilibrium state is achieved, but only if no other disturbance in the cell occurs during this process, which is rarely the case. Figure 1 presents a diagram explaining the above self-interacting ledge dynamics mechanism for the AlF_3 addition.

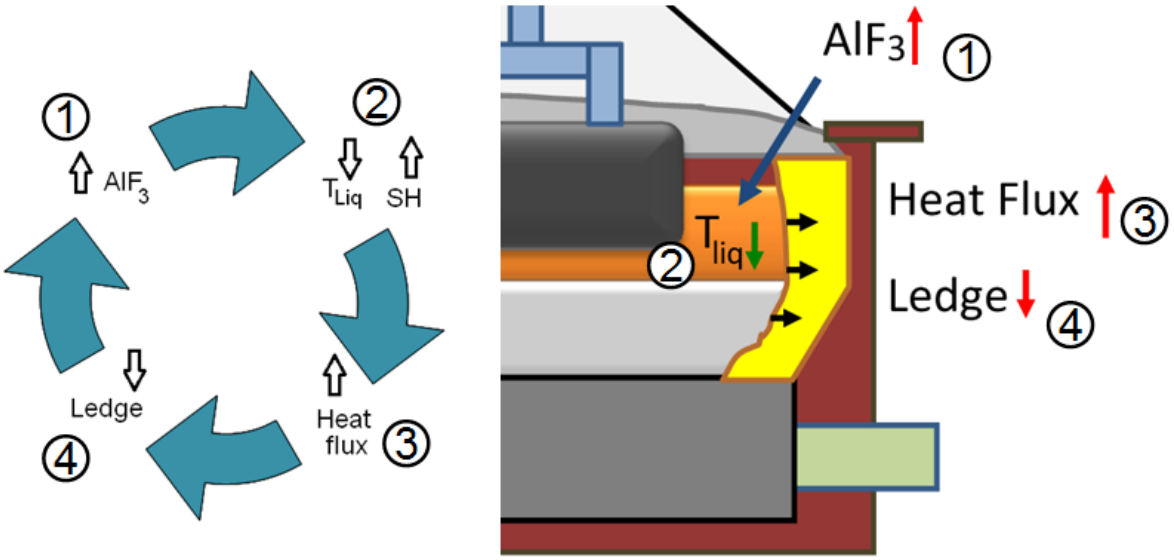

Figure 1: Ledge dynamics, interactions for AlF3 addition (SH=superheat)

A similar process occurs if the disturbance is caused by an energy input variation, as for example, an increase in voltage set point, or rising ACD. More heat is generated inside the bath layer and the superheat increases. The heat dissipation through the cell walls increases, melting part of the freeze. As ledge thickness decreases, AlF_3 concentration lowers due to the bath volume increase, bath melting temperature (*T liquidus*) increases and some freeze forms back until a new equilibrium state is achieved.

The impact of a few different types of energy imbalances on resulting AlF_3 concentration can be found in the literature [9]. The control of the mass and energy balances within an acceptable band of variation has been one of the major challenges of potroom operation. A mathematical model capable of tracking the cell dynamics could help to develop more efficient control routines.

Dynamic Modelling of Mass and Energy Balance

In 2011, an averaged steady state energy balance model was presented by the authors [10]. The model considered new control volume [11] and was based on a complete mass balance of the electrolysis cell. The cell dynamic model was built on the extrapolation of the previous averaged steady state model. The mass conservation law is applied for each substance:

$$\dot{w}_{in\_i} + \dot{w}_{generated} - \dot{w}_{out\_i} - \dot{w}_{consumed} = 0 \qquad (1)$$

Where $\dot{w}$ is the massflow rate of a substance "i". The list of monitored substances in the mass balance includes: Al_2O_3, Al, Na_2O, CaO, H_2O, AlF_3, CaF_2, Na_3AlF_6, C, CO, CO_2, Na_2CO_3, S, COS, SO_2, N_2, O_2, Ar, HF and $NaAlF_4$. Details on the processes and chemical reactions considered are found in [10] and [17]. After the mass balance is obtained, the energy balance of the cell is then performed:

$$Q_{ac} = V_{Cell} I + \dot{w}_{Al}\left(\sum \dot{m}_{i\_in} H_i(T_{i\_in}) - \sum \dot{m}_{i\_out} H_i(T_{i\_out})\right) - \frac{(T_B - T_{amb})}{R_E} \qquad (2)$$

Where Q_{ac} is heat accumulated inside the cell, V_{cell} is cell voltage, I is the line current, $\dot{w}_{Al}$ is the aluminium production rate, $\dot{m}_i$ is the massflow rate per kg of aluminium of substance "i", H_i is the enthalpy of each substance at temperature T_i, T_{amb} *is* the ambient temperature, T_B is the bath temperature and R_E is the equivalent thermal resistance of the cell from the bath to the exterior. Again, the previous published work is recommended for details on each term of equation 2 [10, 17]. In order to study the cell transient dynamics, it is necessary to incorporate a special code using the Finite Volume Method capable of tracking the ledge/bath thermal and chemical interactions, bath volume variation, and also including the heat accumulation effects of the other cell solid volumes.

Ledge Movement: Governing Equations and Boundary Conditions

Figure 2 presents the schematic view of the cell walls calculation domain, where different materials are represented. The shell, insulation/refractory bricks are considered as fixed geometry, whereas the ledge is a deformable geometry. At the surfaces exposed to the potroom environment, the heat dissipation condition is applied via correlations found in the classical heat transfer literature [12] for vertical walls (convection) combined with radiation heat transfer laws.

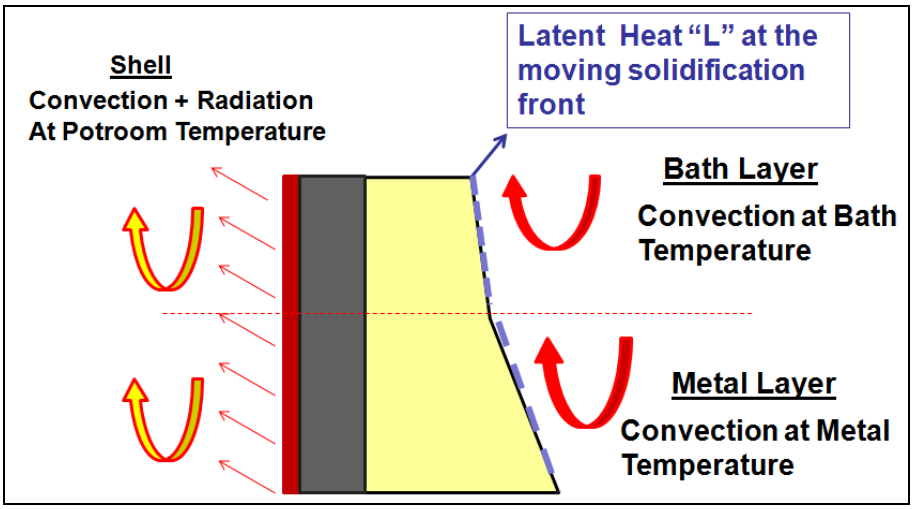

Figure 2: Boundary conditions applied to the dynamic ledge calculation

At the ledge-liquids interfaces, convective heat transfer is applied. Two different treatments are considered for the metal level and bath level as described previously [13]. The energy of

the phase transformation (latent heat) must be included at the ledge boundary, as a local energy source or sink.
The differential equation solved by the numerical method is the energy transport equation where the advective term represents the temperature transport by the grid movement at the ledge domain, see equation 1. The moving grid approach was successfully used earlier by some researchers [8, 14].

$$\rho(x,t)c_P(x,t)\frac{\partial T}{\partial t} - K(x,t)\frac{\partial x}{\partial t}\frac{\partial T}{\partial x} = \frac{\partial T}{\partial x}\left(K(x,t)\frac{\partial T}{\partial x}\right) \qquad (3)$$

Where ρ is density of materials, *cp* is the specific heat capacity of materials, *K* is the thermal conductivity of materials, *T* is the temperature at the grid points, *x* is the grid point position and *t* is the time.
At the cell external walls, the following boundary condition is applied, which takes into account convection and radiation at external surfaces:

$$K(x,t)\frac{\partial T}{\partial x} = h_{ext}(T - T_{amb}) + \sigma\varepsilon(T^4 - {T_{amb}}^4) \qquad (4)$$

Where h_{ext} is the shell wall heat transfer coefficient, T_{amb} is the potroom temperature, σ is the Stefan-Boltzman constant for radiation and ε is the shell emissivity.
The boundary conditions applied at the ledge-bath interface (equation 5) and ledge-metal interface (equation 6), present an extra term representing the melting/solidification latent heat.

$$\rho(x,t)L\frac{\partial x}{dt} + h_b(T_B - T_L) = K(x,t)\frac{\partial T}{dt} \qquad (5)$$

$$\rho(x,t)L\frac{\partial x}{dt} + h_m(T_m - T_L) = K(x,t)\frac{\partial T}{dt} \qquad (6)$$

Where *L* is the latent heat, T_B is the bath temperature, T_m is the metal temperature, T_L is the *liquidus* temperature of the bath, h_b is the bath/ledge heat transfer coefficient and h_m is metal/ledge heat transfer coefficient.
In addition to the previous boundary conditions, the solidification front temperature is equal to the *liquidus* temperature:

$$T = T_L \qquad (7)$$

The *liquidus* temperature is obtained from the bath composition [15], which is evaluated at each time step taking into account the mass balance [10] of the cell and the bath volume.
The energy equation is transient and necessitates the initial condition for all grid points.

$$T = T(x,0) \qquad (8)$$

Solution Algorithm

The computational dataflow chart of the dynamic model is shown in Figure 3. Usually, it is recommended starting the dynamic simulation from a converged steady state solution because this is a numerically more stable situation. It is possible, however, to start the transient calculation from a transitory cell state, provided the initial heat fluxes and energy or mass accumulation rate are known. Inside each time step, mass balance, energy balance, ledge position, bath volume, bath composition, bath temperatures and the superheat are interlinked and calculated simultaneously. The method is iterative and numerical convergence must be achieved for each time step, before the next time step calculation starts.

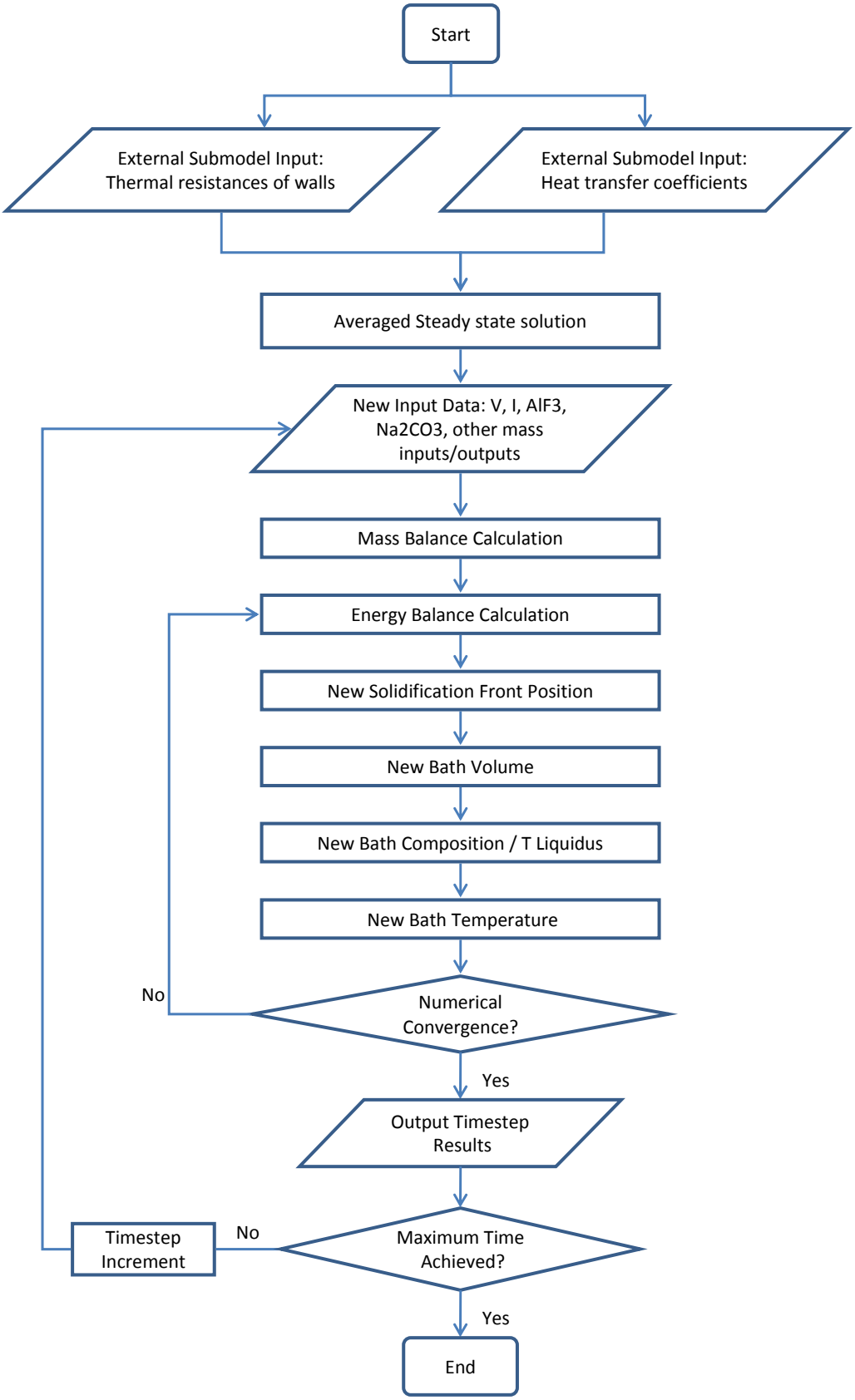

Figure 3: Computational flowchart of the dynamic model algorithm

A moving grid technique is adopted to track the solidification/melting front. The Finite Volume Method was chosen to calculate the transient ledge energy equation and movement [16]. The moving grid algorithm of the ledge movement was tested for mesh independence,

time step independence and iteration convergence, as detailed in reference [17]. Because the simulations are transient, the appropriated time step size must be chosen according to the process to be studied. For mass balances disturbances such as alumina feeding, small timescales are required (~1s), whereas for energy input variations such as power modulation, greater timescales can be used (5-10min).

Power Modulation Study

In some regions of the world, where electrical energy is now a scarce resource, the energy tariffs may vary depending on the time of the day in a 24h cycle, aiming to encourage consumption during the low demand period and to reduce consumption during the demand peaks. This opens the opportunity for smelters to modulate the power inputs in order to decrease the averaged energy cost.

Power modulation has been applied by smelters with reported success [18-20]. Stam and Schaafsma [20] tested different power modulation setups at Aluminium Delfzijl reporting some difficulties during the low energy input period: excessive freeze of bath, low superheat with consequential poor alumina dissolution. After a long power modulation period, the cited smelter reported deterioration of the controllability of the bath levels, bottom ridging, metal quality decrease, anode spike occurrence due to low temperature/superheat. Despite all these inconvenient outcomes, important reductions in power cost were reported. More recently, several tests have been carried out at TRIMET Hamburg [21] in order to determine the effect of increased or decreased energy input to the cells, and as well as the time necessary for the cell to return to stable conditions.

With the help of the cell dynamic model, it is possible to investigate the impact of power modulation in the cell transient behaviour through virtual testing. In the model, the power input is applied at each time step, following the modulation function, and the resulting perturbations are obtained. Bath temperature, bath chemistry, ledge thickness and wall temperatures are monitored during the simulation.

In order to demonstrate the dynamic model capabilities, two different modulation functions are applied to the model as shown in Figure 4 and Figure 5. The general assumptions adopted for this study are:

- Averaged line current is 180.7 kA. Modulation amplitude is 20 kA in a 24 h period.
- No other transient effects are included.
- The cell voltage remains unchanged during this simulation.
- Time step size: 360 s.
- Ledge is composed of pure cryolite composition ($3NaF*AlF_3$).

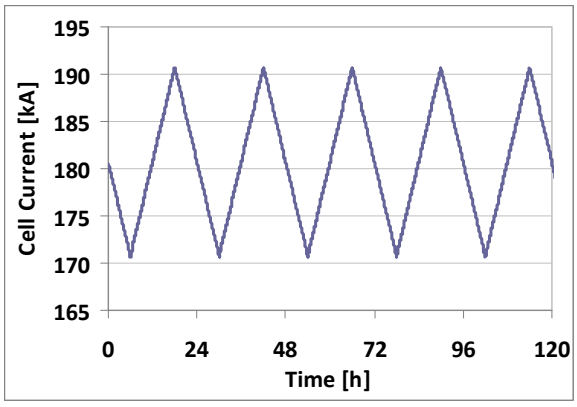

Figure 4: Cell current input. Linear modulation function.

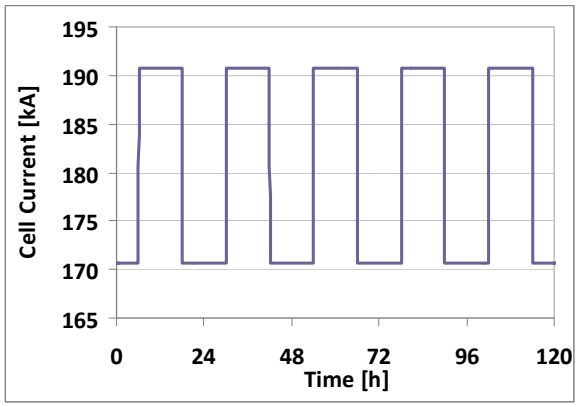

Figure 5: Cell current input. Stepped modulation function.

The calculated ledge thickness oscillations for both modulation setups are presented in Figure 6 and Figure 7. Ledge movement is monitored in four calculated representative points: at the sidewall metal level, sidewall bath level, endwall metal level and endwall bath level.

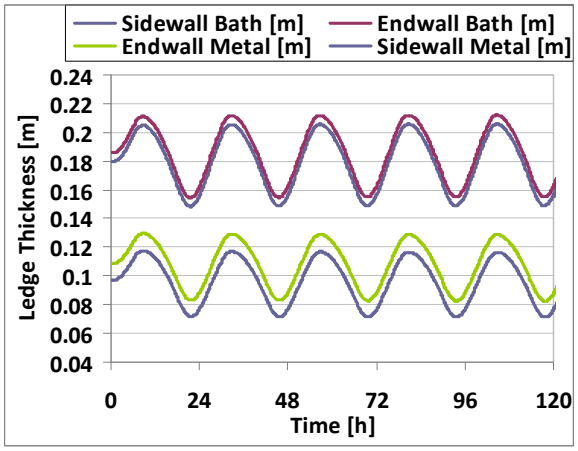

Figure 6: Calculated ledge thickness at four different locations. Linear modulation function.

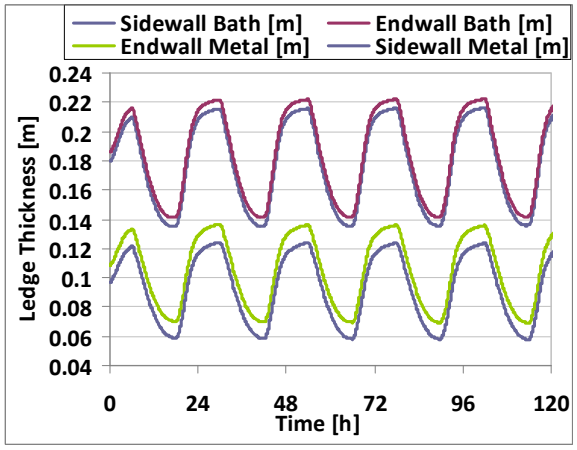

Figure 7: Calculated ledge thickness at four different locations. Stepped modulation function.

The ledge movement amplitude is higher (around 8 cm against 6 cm) when the cell is under the stepped power modulation. This outcome might be explained by the fact that the stepped function presents higher power variance around the average compared with the linear function.

The energy input oscillations would also be manifested at the shell external temperatures. The Figure 8 and Figure 9 present the calculated temperature in four key locations of the shell (sidewall metal level, sidewall bath level, endwall metal level and endwall bath level), during five days of power modulation.

Temperature variation amplitudes up to 20 Celsius degrees are observed (stepped power input case). Higher temperature variations are found at the bath level. The thermal resistance of the cell insulation is typically lower at the bath level than the resistance at the metal level, explaining why the temperature is more sensitive to cell disturbances at that location.

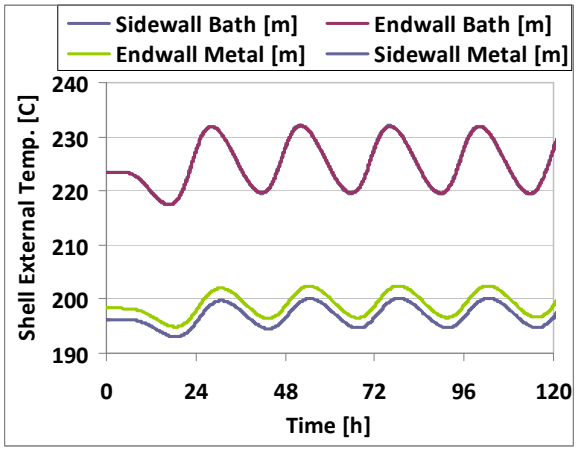

Figure 8: Calculated shell external temperature at four different locations. Linear modulation function.

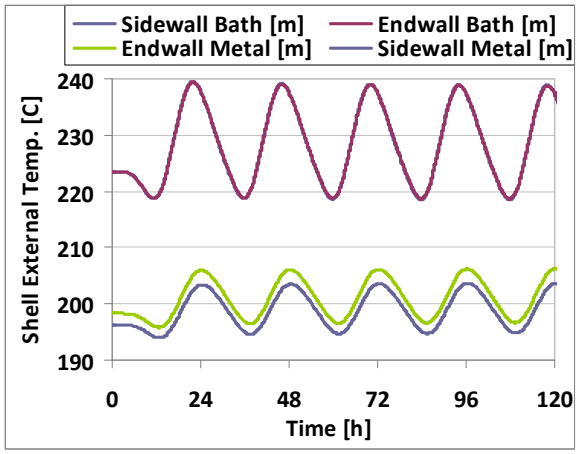

Figure 9: Calculated shell external temperature at four different locations. Stepped modulation function.

Because the simulation starts from a steady state solution, and the heat wave takes many hours to navigate from the internal liquids through the refractory/insulating materials, the shell temperatures remained nearly constant during the initial hours of the process.

Figure 10 and Figure 11 show the variation in the aluminium fluoride concentration of the bath caused by ledge melting/solidification during the power modulation cycle.

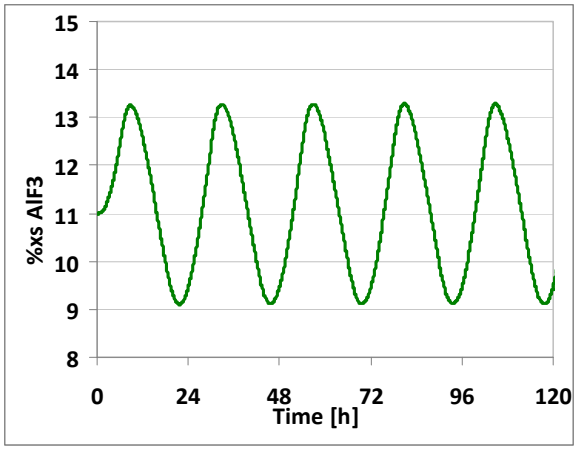

Figure 10: AlF_3 %wt oscillation produced by the linear modulation function.

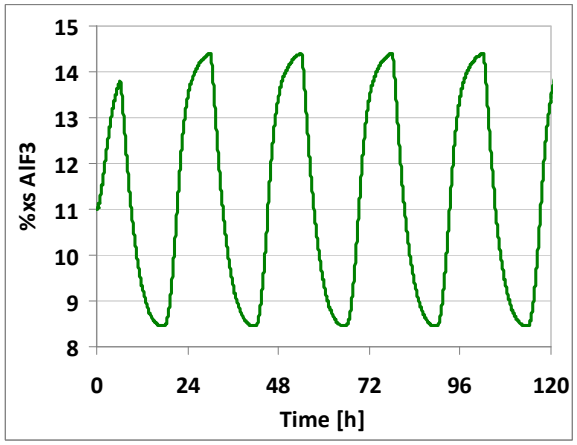

Figure 11: AlF_3 %wt oscillation produced by the stepped modulation function.

The linear modulation function produced ~4% variation in excess AlF_3, while the stepped function resulted in ~6% variation. This difference is significative when focusing the bath chemistry control. The bath superheat is impacted both by the energy input wave and the bath composition oscillation resulting in the graphs of Figure 12 and Figure 13.

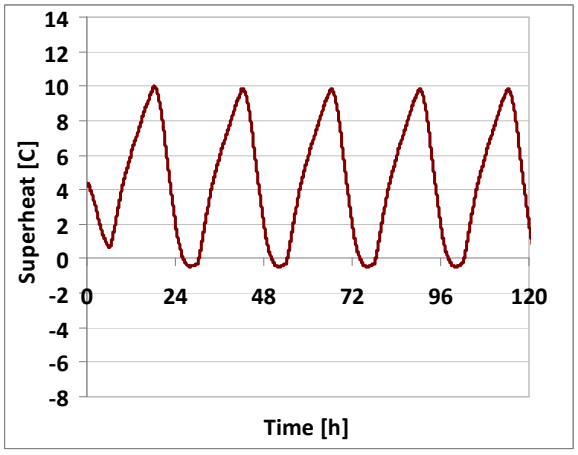

Figure 12: Superheat oscillation produced by the linear modulation function.

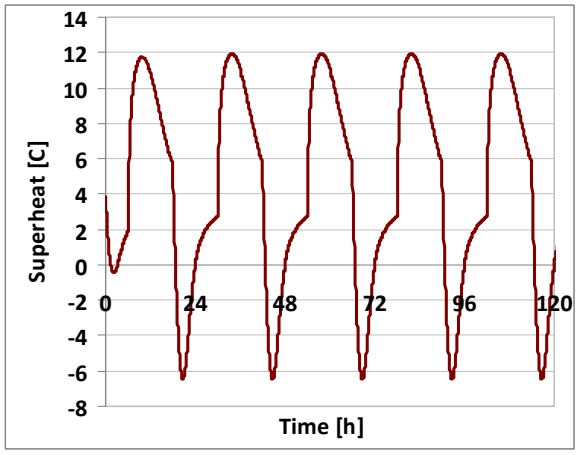

Figure 13: Superheat oscillation produced by the stepped modulation function.

In the model, negative superheat is sometimes observed, mainly in the stepped modulation case. In industrial cells, this would probably be manifested as solidification of bath over the cathode blocks and/or sludge formation, because the alumina needs a few degrees of superheat to heat up and to dissolve.

Figure 14 and Figure 15 present the relationship between fluoride concentration and bath temperature obtained at each time step in the dynamic simulations, plotted in the temperature *versus* AlF_3 concentration space, as used earlier by Taylor and Welch [22].

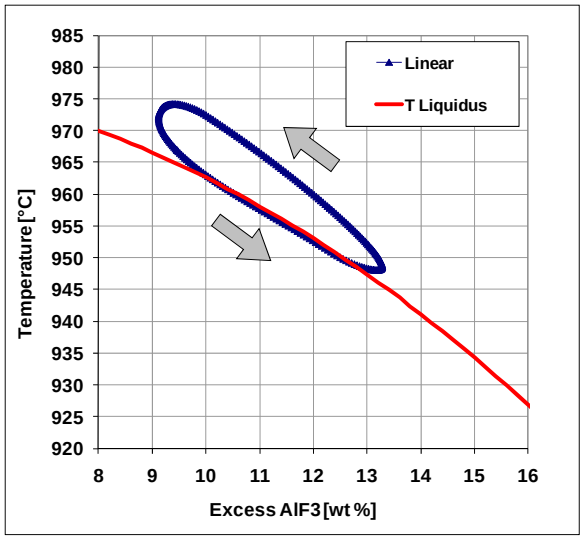

Figure 14: Bath temperature/AlF_3 concentration diagram for calculated cell states. Linear modulation function.

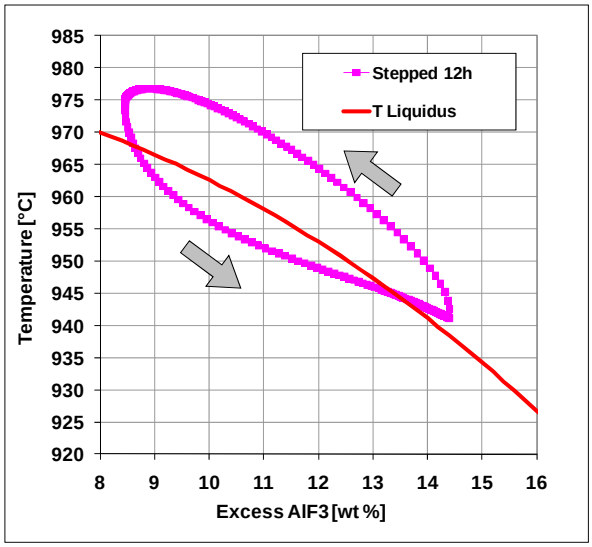

Figure 15: Bath temperature/AlF_3 concentration diagram for calculated cell states. Stepped modulation function.

The power modulation is a cyclical process, thus the behaviour of bath temperature/AlF_3 is repeated at each period. Here, one period of 24h is represented. In the linear modulation case, the trajectory of cell states is restrained by a smaller cycloid area. The movement is always counter clockwise in the graphs due to the nature of the process.

Delay of Thermal Response to Power Modulation

As previously noted, the heat wave takes many hours to travel inside the cell lining, this delay is in the order of magnitude of the periodic energy disturbances: anode change, fluoride additions, metal tapping, causing any cell in the industry to remain in a continuous thermal transient state, even when the electrical energy input is constant. In the next graphs (Figure 16 and Figure 17) a direct comparison is made by simultaneously plotting the cell current modulation function with the ledge thickness and with the shell temperature (both sidewall bath region) for the studied modulation cases.

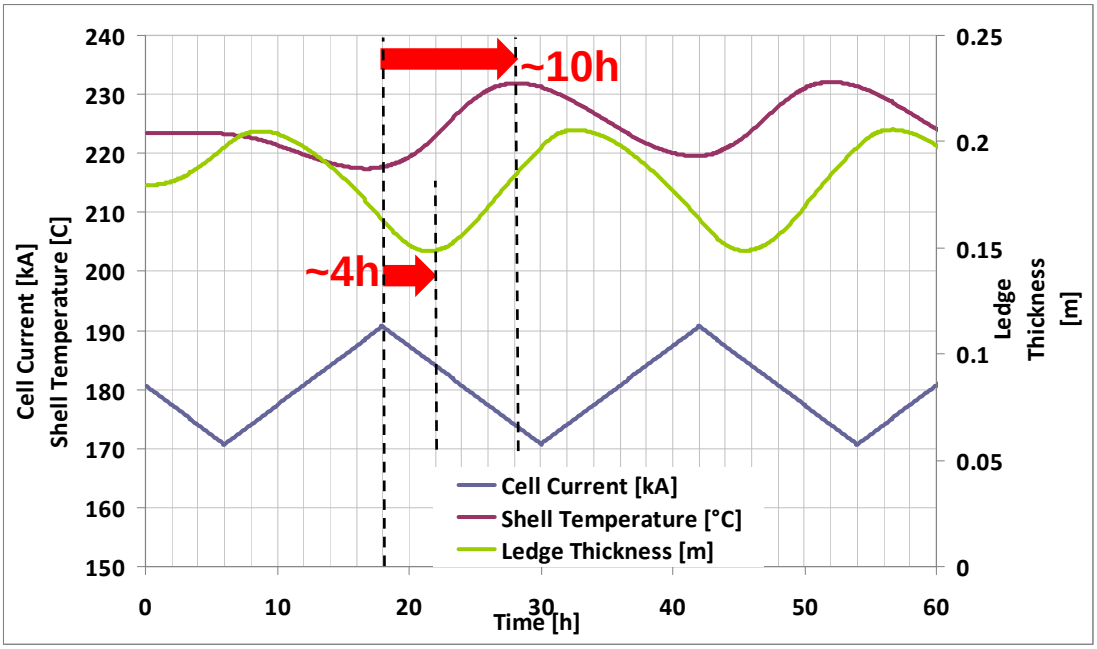

Figure 16: Power modulation curve *versus* ledge thickness *versus* shell external temperature. Linear modulation function.

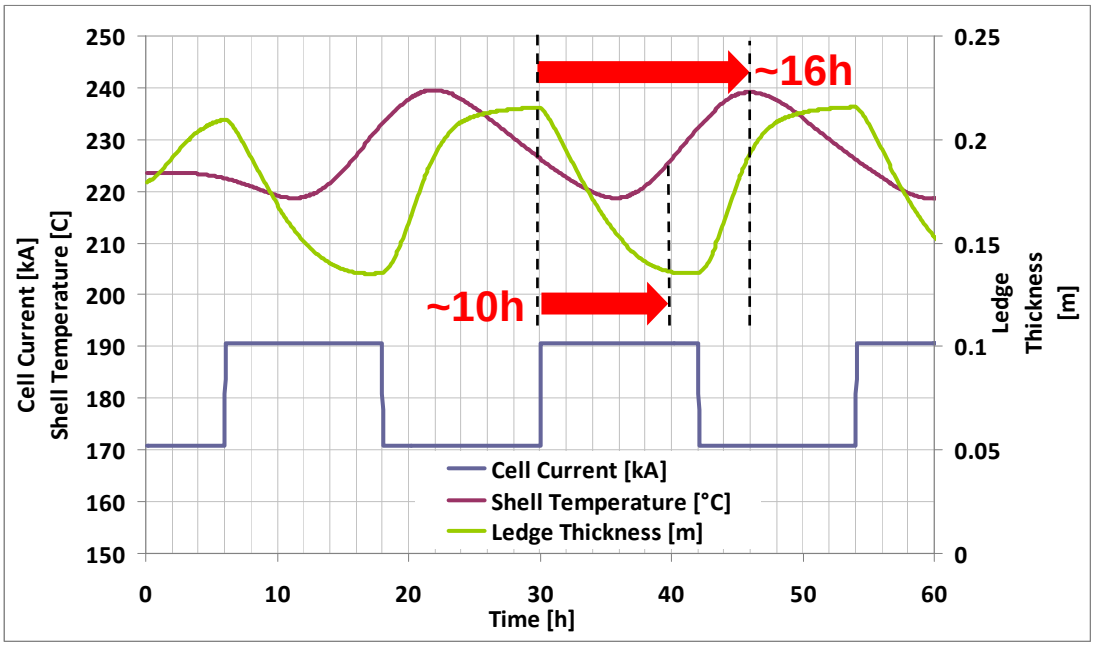

Figure 17: Power modulation curve *versus* ledge thickness *versus* shell external temperature. Stepped modulation function.

In the linear modulation case, if we adopt the peak value for the electrical energy input rate as the reference point, the results show that the ledge thickness takes approximately 4 hours to reach its minimum thickness. Moreover, the shell temperature would reach its maximum temperature only 10 hours after the energy input peak and 14 hours before the next energy input peak, almost reaching a perfect negative phase between the oscillation curves.
In the stepped modulation case, if we choose to consider the starting of the maximum energy input as the reference point, the ledge reaches the approximated minimum thickness after 10 hours and the shell temperature maximum occurs only after 16 hours.

Fluoride Additions

The bath composition control is very important to obtain efficient cell operation. The bath properties are sensitive to AlF_3 concentration, which is gradually consumed mainly by two mechanisms.

a) Neutralisation of Na_2O and CaO present in the alumina as impurities;
b) Evaporation of gaseous fluorides HF and $NaAlF_4$.

The consumption rate of mechanism (a) can be considered constant. The consumption rate by emissions (b) might be considered constant, except during anode change procedures or any other procedure requiring the cell top to be open. In the modern industry, up to 99% of fluoride emissions are recycled and come back into the bath together with the reacted alumina. Nowadays the net consumption by mechanism (b) is much smaller than by mechanism (a).
In order to control the bath composition and properties, AlF_3 is periodically added to maintain balance. In many cell technologies, this procedure is done by dissolving a certain amount of AlF_3 in the bath once a day. Recent technologies present a special AlF_3 feeder, which makes the fluoride correction closer to continuous addition.
In this section, the cell behaviour disturbances caused by the AlF_3 additions are investigated using the dynamic model. The fluoride consumption rate is assumed to be constant in time, and the corrective addition occurs each 24h. The addition mass is calculated to be equal to the one day's consumption (22.85 kg) in this case. All other cell disturbances are neglected in this study.

The fluoride addition triggers a sequence of events, as described in Figure 1:

- AlF_3 addition and dissolution;
- *T liquidus* decreases at higher AlF_3 excess, consequently superheat increases;
- Cell wall heat flux increases;
- Ledge melts down;
- AlF_3 concentration decreases as bath volume increases;
- After enough time, the equilibrium concentration would become lower than immediately after the addition because the bath volume increased;

The next results represent a simulation of 5 days of process, where 5 fluoride additions took place. Figure 18 shows the excess AlF_3 inside the bath during the process (in mass), while Figure 19 shows the corresponding fluoride concentration, in weight percent, calculated by the dynamic model.

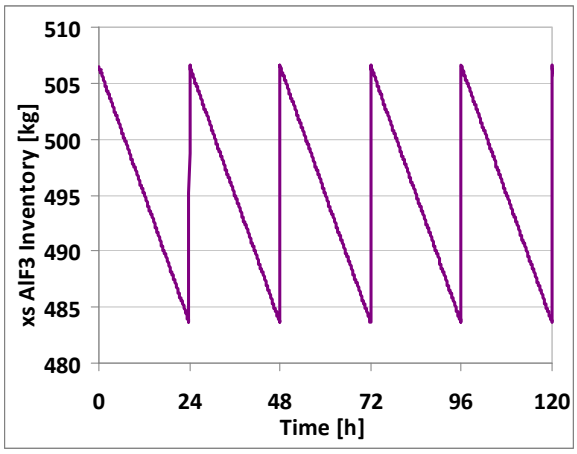

Figure 18: Excess AlF3 mass inventory, one addition per day to compensate the fluoride total consumption.

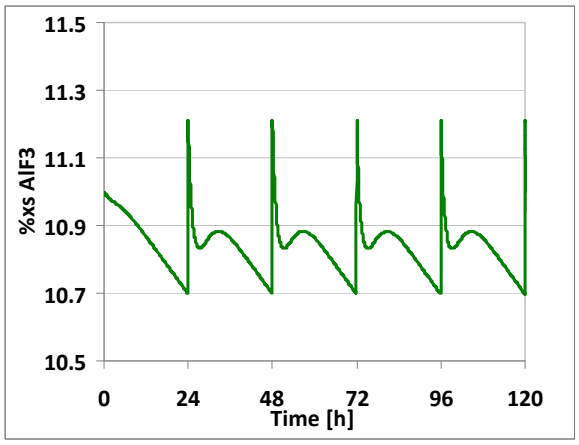

Figure 19: Excess AlF3 (weight %), one addition per day to compensate the fluoride total consumption.

The % excess AlF_3 graph of Figure 19 combines the variation effects of two phenomena:

- $\%AlF_3$ decreases, by continuous consumption to neutralise Na_2O, CaO, and HF evolution.
- The bath volume variation caused by the ledge melting/solidification affects the $\%AlF_3$. Sometimes, it is observed in the results that the bath volume is decreasing, increasing the % excess AlF_3 at a faster rate than its regular consumption.

The fluoride additions cause a variation in the liquidus temperature of approximately 2.5 °C, impacting the bath superheat in the same order of magnitude, see Figure 20. This represents an important disturbance in the cell heat balance, as the heat dissipation through the sidewalls is controlled by the bath superheat, ideally ranging from 5°C to 10°C.

In Figure 21, the total heat flow at the ledge solidification front is compared with the heat dissipation at the shell, both at the sidewall bath level. The superheat peaks caused by the fluoride additions are reflected in the heat input peaks at the ledge. The heat output at the shell presents much smaller variation amplitude because of the heat diffusion damping. In an averaged steady state simulation, both values would be always equal. These results show that AlF_3 additions strongly impact the cell energy balance dynamics.

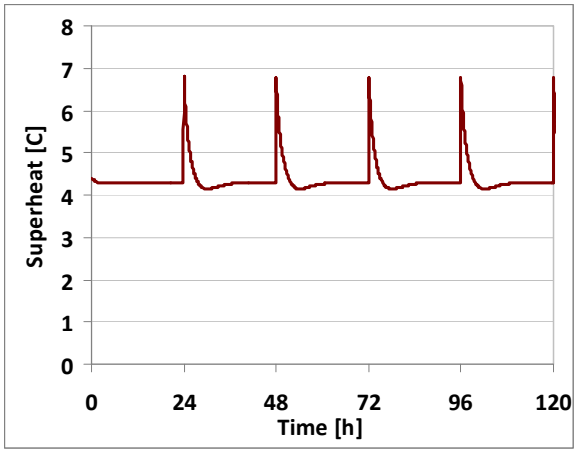

Figure 20: Calculated bath superheat. Bath correction: one addition per day to compensate the fluoride total consumption.

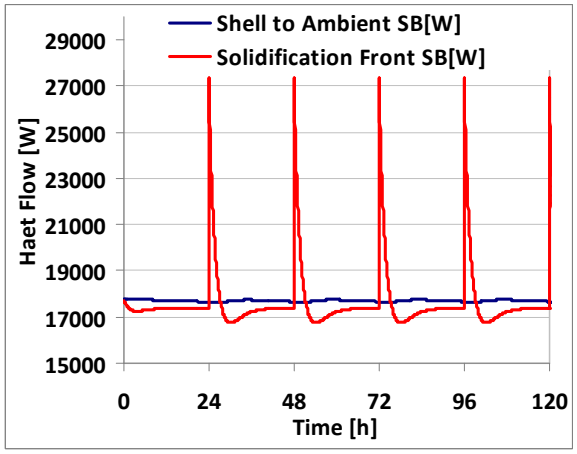

Figure 21: Comparison of ledge heat input *versus* the shell to ambient heat output. Both at sidewall bath region (SB)

Simulation Using Real Cell Data Input

The dynamic model is capable of reading a text file containing: voltage *versus* time, line current *versus* time and AlF_3 addition *versus* time. The program applies all these values at the specified times as mass and energy inputs. Data obtained from industrial cells can be inserted into the model and the dynamic behaviour of a particular cell can be analysed. Many virtual tests can be performed regarding bath temperature and composition control. In the results, it is possible to foresee the dynamic consequences of those inputs on bath temperature, superheat, $\%AlF_3$, ledge thickness and shell temperature.

As an example, Figure 22 shows the bath temperature obtained by the dynamic model for the cell using the industrial inputs for voltage, current and fluoride additions, compared with the temperature measured by the smelter. All relevant cell geometry data and material properties were also provided, in order to set up the dynamic model. Some limitations of the simulation and the comparison must be remembered when interpreting the results:

- Voltage and cell current inputs are an average of 24h of process;
- AlF_3 addition occurs once a day;
- Calcium fluoride concentration was considered constant during the simulated period;
- Temperature measurements were usually taken at each two days by the smelter operational staff; many values were repeated in order to obtain a plot with one point at each 24 h. In the dynamic model, the temperature is recalculated each 6 minutes of process;
- The model does not consider anode changing disturbances;
- The bath temperature measurements done in real cells have some reliability limitations as discussed elsewhere [23]. It is normally a manual process subjected to several sources of error, such as:
    - Variation in the depth of immersion of the sensor;
    - The crust must be broken and the bath is exposed, cooling the bath locally;
    - Spatial temperature variations inside the bath, caused by the setting of new cold anodes.

Despite the errors listed above, reasonable agreement between measurements and dynamic simulation was obtained (Figure 22).

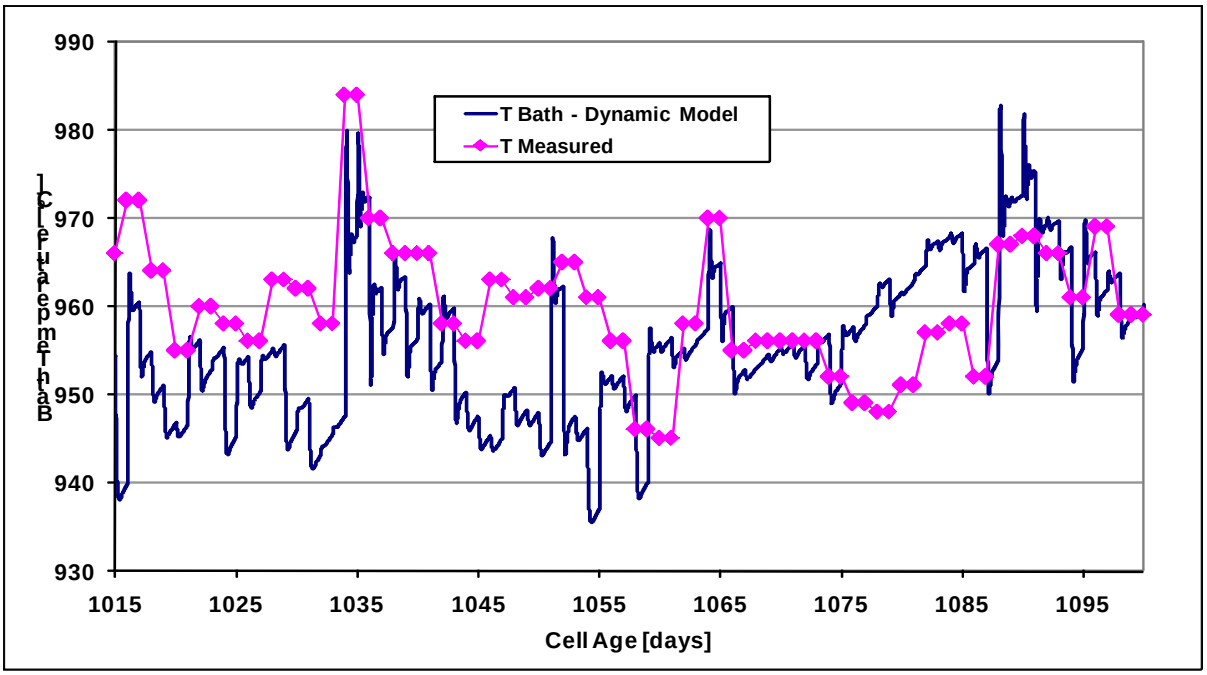

Figure 22: Comparison between measured and calculated bath temperatures during 85 days of process.

The bath temperature oscillations are correlated with the cell power input and as well the bath composition variations, which determines the solidification temperature of the ledge.

The measured cell states are plotted on the temperature *versus* AlF_3 operational window presented in Figure 23. The desired operational region is defined by the green polygon. Figure 24 presents the calculated cell states for the same time frame.

In the measured values diagram, it is observed that the cell is floating from low to high superheat on many occasions; in one opportunity very high superheat is found, more than 30°C while in other moments, low or even negative superheat is found. Many points are found outside the optimum operational window (green polygon). This is caused either by AlF_3 imbalances or by energy imbalances produced by power input variations.

The same behaviour is found in the diagram obtained by the dynamic model simulation. In the model, many more points can be calculated and plotted turning the tracking of cell states into a continuous line. The fluoride additions can be identified as straight line "jump" towards the positive "x" coordinate direction. The bigger cell temperature excursions are represented by the longer cycloid curves leading to important modifications in the cell state.

Many points are located outside the green optimal window, as observed also in the measurements graph. Again, it is possible to identify moments when the superheat is negative (below the red line) and moments when the superheat achieves values higher than 25°C. In the model, the range of cell states defined by the blue line trajectory is wider than is found in the measurements within the same timeframe. Such a difference might be expected because the low measurements frequency is not capable of obtaining the whole cell excursion behaviour.

The existence or not of negative superheat in the cell has been discussed in the literature [24], and might be a product of measurement errors in bath sample compositions [25]. According to Kvande [26], the values measured by the superheat probes are always positive. Possibly, the sludge precipitation occurring at low superheat periods is capable of maintaining superheat values always positive. This effect is not implemented yet in the present dynamic model.

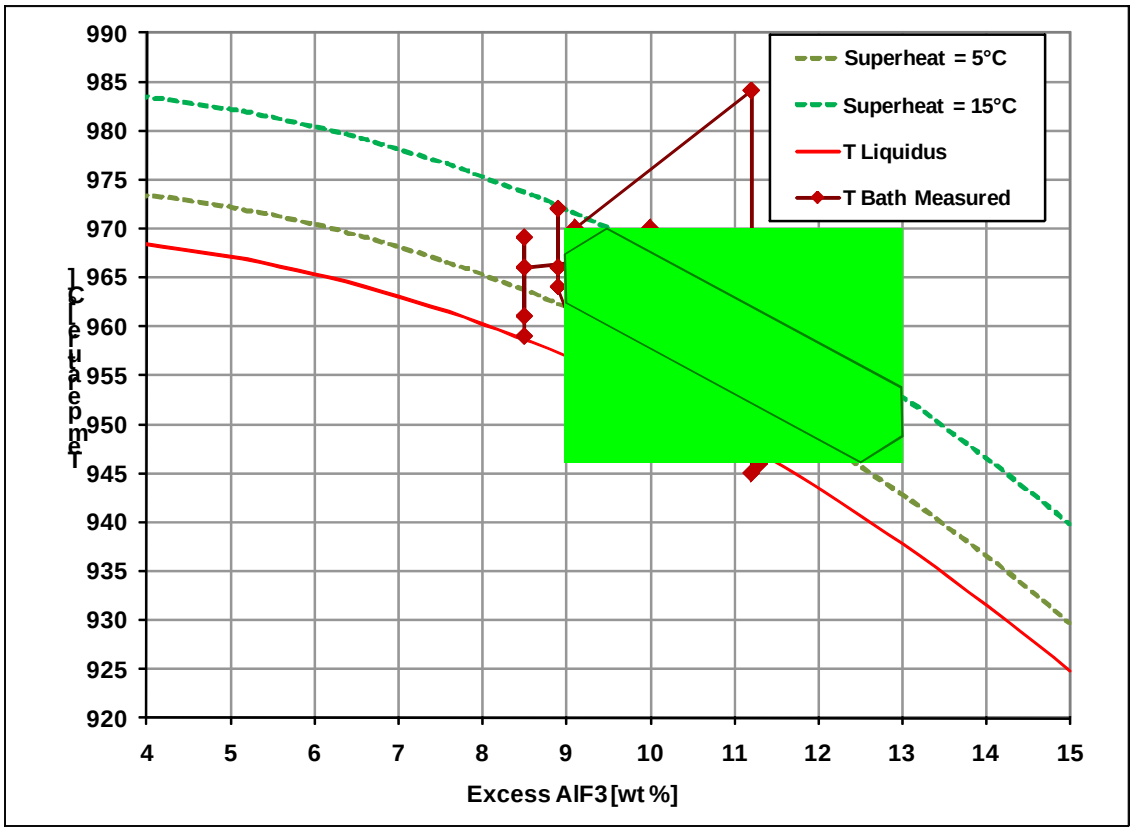

Figure 23: Measured bath temperature *versus* % AlF3 state in the cell compared with the optimal bath chemistry window.

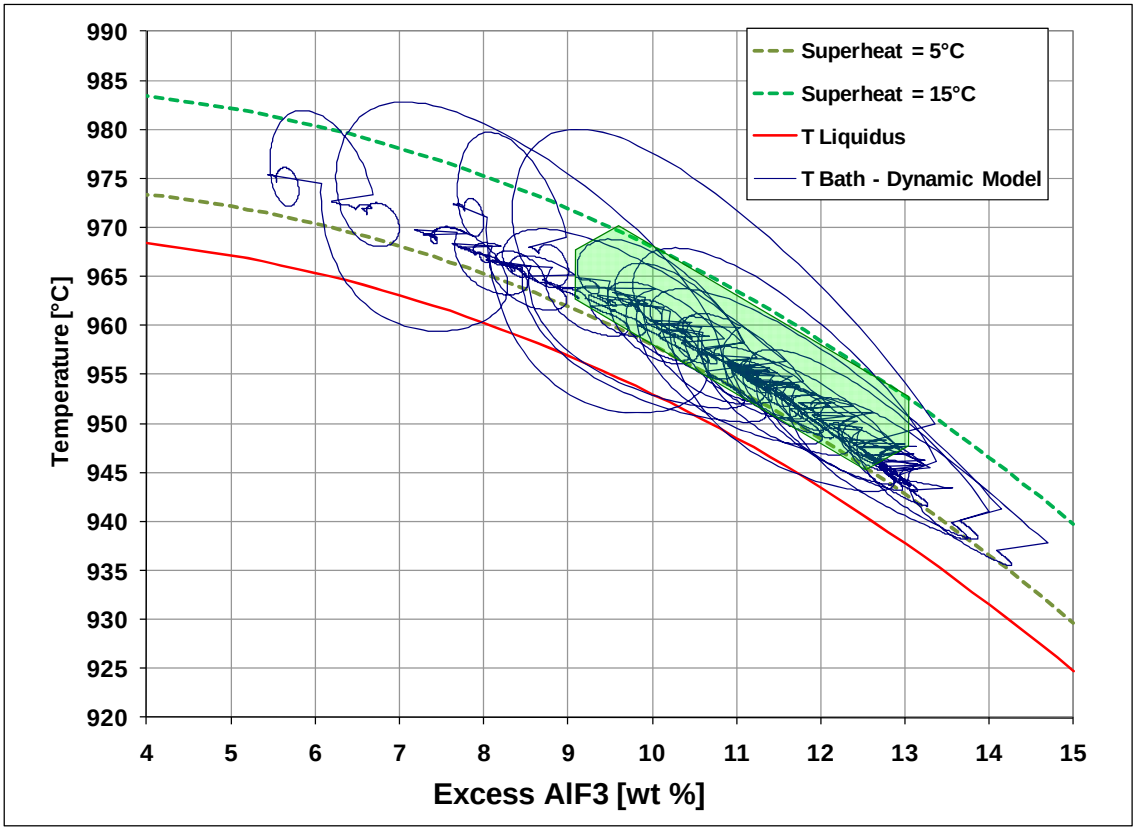

Figure 24: Calculated bath temperature *versus* AlF3 (wt %) for the same measured case, using the voltage, current and AlF_3 inputs reported by the smelter.

Conclusions

The cell dynamic model presented in this work is a valuable tool for improving the understanding of the complex interactions between the mass balance and energy balance of aluminium electrolysis cells. The consequences of each particular cell disturbance on both balances can be assessed by virtual testing. The model results can be used to potentially improve the process control, and actions to stabilise the cell behaviour can be developed.

In general, existing cell heat balance models and measurement routines describe the cell instantaneous thermal state but neglect the previous cell thermal excursion paths. Because of the ledge solidification front movement and the heat capacitance of the materials, the past imbalances and perturbations will affect the future cell behaviour. The present dynamic model posses the features necessary for tracking the transient nature of the electrolysis cell operation.

The dynamic model was employed to study the impact of the power modulation on the Hall-Héroult cell behaviour. Two types of power modulation curves were simulated. The results show the advantage of applying the linear function due to its lower variation on the energy balance of the cell. The model can be used to develop process control countermeasures, aiming to compensate the power modulation energy input wave with some kind of variation in the cell energy output.

The impact of AlF_3 additions on the transient cell energy balance stability was studied. It was shown that the bath superheat presents a significative perturbation after the addition, causing melting of ledge and energy balance readjustment. In many smelters, aluminium fluoride additions are used not only to control the bath chemistry, but also to control the bath temperature. Such a procedure may induce strong cell thermal excursions due to the mass imbalance instead of stabilising the cell bath chemistry and energy balance. Cell thermal imbalances should be treated with readjustments on heat generation and on heat losses while chemical imbalances should be treated with the appropriated mass balance. Only with a very good measurement routine and with the help of dynamic models, it is possible to differentiate a thermal imbalance from a chemical imbalance in an operating electrolysis cell.

Finally, the model was also employed to simulate the industrial cell behaviour under cell data inputs. The cell thermal excursions found in the model results are of considerable magnitude, potentially harming the freeze protective layer. Overestimation of fluoride addition mass by the cell control routine is also responsible for sudden increases in superheat.

Future Research

The analysis of the anode effect impact on the cell energy balance would be an interesting feature to be implemented in the model, which would help the industry to control the anode effect impact on energy consumption and PFC gas emission rate. However, in order to accomplish this task, the mass balance would have to include the PFC gases as possible products of the process. Additional inputs regarding the anode effect parameters such as AE duration, frequency and voltage including a predicted decrease in current efficiency would have to be specified at the start of the simulation.

In addition to the capabilities of the dynamic model presented in this paper, the ultimate goal of the model development would be its integration with the industrial cell control system and

the potline control practices. The control system and human decisions could be supported by modelling predictions.

References

1. J. N. Bruggeman, D. J. Danka, “Two-Dimensional Thermal Modeling of the Hall-Heroult Cell”, *TMS Light Metals 1990*, pp 203-209.
2. M. Dupuis, “Computation of Aluminum Reduction Cell Energy Balance using ANSYS ® Finite Element Models”, *TMS Light Metals 1998*, pp 409-417.
3. I. Tabsh, M. Dupuis, A. Gomes, “Process Simulation of Aluminum Reduction Cells”, *TMS Light Metals 1996*, pp 451-457.
4. T. Hashimoto, H. Ikeuchi, “Computer simulation of dynamic behavior of an aluminum reduction cell”. *TMS Light Metals 1980*, 273-283.
5. L. Tikasz, R. T. Bui, V. Potocnik, “Aluminium Electrolytic Cells: A Computer Simulator for Training and Supervision“, *Engineering with Computers (1994)* 10:12-21, Springer-Verlag London Limited, 1994.
6. M. P. Taylor, W. D. Zhang, V. Wills, S. Schmid, “A Dynamic Model for the Energy Balance of an Electrolysis Cell”, *Transactions of the Institution of Chemical Engineers, Volume 74, Issue 8, November 1996*, Pages 913-933.
7. T. Drengstig, “On Process Model Representation and AlF3 Dynamics of Aluminum Electrolysis Cells” *Dr. Ing. Thesis, Department of Engineering Cybernetics - Norwegian University of Science and Technology*, Trondheim-Norway, August 1997.
8. A.G. Barantsev, V.V. Yurkov, V.C. Mann, T.V. Piskazhova, K.F. Nikandrov, “Model of Process of Electrolyses”, *TMS Light Metals 2000*, pp. 315–321.
9. B. J. Welch, “The Impact of Changes in Cell Heat Balance and Operations on the Electrolyte Composition”, *6th Australasian Aluminum Smelting Workshop Proceedings*, Queenstown, New Zealand, 22-27th November 1998, pp 191-204.
10. V. Gusberti, D. S. Severo, B. J. Welch, M. Skyllas-Kazacos, ―”Modelling the Aluminium Smelting Cell Mass and Energy Balance – a Tool Based on the 1st Law of Thermodynamics”, *10th Australasian Aluminium Smelting Technology Conference,* Launceston, Australia, 10th-14th October 2011.
11. B. J. Welch, J. T. Keniry – “Advancing the Hall-Heroult Electrolytic Process”, *TMS Light Metals* 2000, pp 17-26.
12. F. P. Incropera, D. P. De Witt, “Fundamentals of Heat and Mass Transfer”, *2nd edition 1985 - John Wiley and Sons,* New York, USA.
13. D. S. Severo, V. Gusberti, "A Modelling Approach to Estimate Bath and Metal Heat Transfer Coefficients", *TMS Light Metals 2009*, pp 557-562.
14. C. C. Wei, J. J. J. Chen, B. J. Welch, B. R. Voller, “Modelling of Dynamic Ledge Heat Transfer”, *TMS Light Metals 1997*, pp 309-316.
15. A. Solheim, S. Rolseth, E. Skybakmoen, L. Stoen, A. Sterten, T. Stoere, “Liquidus Temperatures for Primary Crystallization of Cryolite in Molten Salt Systems of Interest for Aluminum Electrolysis*”, Metallurgical and Materials Transactions B - Volume 27B* - October 1996, pp 739-744.

16. S. V. Patankar, “Numerical Heat Transfer and Fluid Flow”, *McGraw Hill,* New York. 1980.
17. V. Gusberti – Modelling the Mass and Energy Balance of Aluminium Reduction Cells, *School of Chemical Engineering, Faculty of Engineering, UNSW. PhD Thesis Awarded by: University of New South Wales*, Sydney-Australia, 2014.
18. L.J.P.L. Nunes, , A. V. da Silva, L.F. G. Soutinho, , “Power Modulation on Valesul P-19 Pots”, *TMS Light Metals 1998*, pp. 1267-1271.
19. E. Kuhn, N. Malcolm, “Power Modulation within ALCOA’s Warrick Operations”, *TMS Light Metals 2009*, pp 323-326.
20. M. A. Stam, J. Schaafsma, “The Impact of Power Modulation on the Cell Dynamics”, 9th *Australasian Aluminum Smelting Conference and Workshop Proceedings*, Terrigal, Australia, 4-9th November 2007.
21. T. Reek, “A Novel Approach to Power Modulation”, *10th Australasian Aluminium Smelting Technology Conference,* Launceston, Australia, 10th-14th October 2011.
22. M. P. Taylor, B. J. Welch, “Improved Energy Management For Smelters”, *8th Australasian Aluminum Smelting Conference and Workshops Proceedings*, Yeppoon, Australia, 3-8th October 2004.
23. D. Whitfield, B. J. Welch, M. Skyllas-Kazacos, “Temperature in Reduction Cells”, *7th Australasian Aluminium Smelting Conference and Workshop Proceedings*, Melbourne, Australia, 11-16th November 2001.
24. W. E. Haupin, “The Liquidus Enigma”, *TMS Light Metals 1992*, pp. 447-480.
25. B. P. Moxnes, A. Solheim, T. Støre, B. E. Aga, L. Støen, “The “Liquidus Enigma” Revisited”. *TMS Light Metals L. 2006*, pp. 285-290.
26. H. Kvande, “A Technological Overview of the Primary Aluminium Industry - Yesterday, Today and Tomorrow” *8th Australasian Aluminum Smelting Conference and Workshops Proceedings,* Yeppoon, Australia, 3-8th October 2004.